R91-917992-2

FATIGUE AND FRACTURE OF INTERMETALLIC ALLOYS

Prepared by

C. V. Cooper
H. R. P. Inoue
A. F. Giamei
L. H. Favrow

ANNUAL REPORT

Contract F49620-89-C-0047

for

Air Force Office of Scientific Research
Bolling Air Force Base
Washington, DC 20332

May 22, 1991

UNITED TECHNOLOGIES RESEARCH CENTER

DISCLAIMER NOTICE

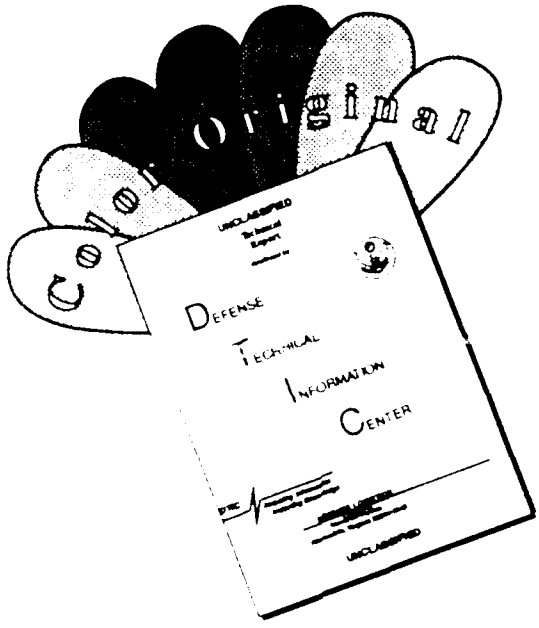

THIS DOCUMENT IS BEST QUALITY AVAILABLE. THE COPY FURNISHED TO DTIC CONTAINED A SIGNIFICANT NUMBER OF COLOR PAGES WHICH DO NOT REPRODUCE LEGIBLY ON BLACK AND WHITE MICROFICHE.

REPORT DOCUMENTATION PAGE

Form Approved
OMB No 0704-0188

1. AGENCY USE ONLY (Leave blank)	2. REPORT DATE	3. REPORT TYPE AND DATES COVERED
	4/30/91	Annual 4/1/90 - 3/31/91

4. TITLE AND SUBTITLE

Fatigue and Fracture of Intermetallic Alloys

5. FUNDING NUMBERS

F49620-89-C-0047

6. AUTHOR(S)

C. T. Cooper, H. R. P. Inoue,
A. F. Giamei, and L. H. Favrow

7. PERFORMING ORGANIZATION NAME(S) AND ADDRESS(ES)

United Tech. Res. Ctr.
400 Main Street
E. Hartford, CT 06108

and

Univ. of Illinois
at Urbana-Champaign
Urbana, Illinois 61801

8. PERFORMING ORGANIZATION REPORT NUMBER

R91-917992-2

9. SPONSORING/MONITORING AGENCY NAME(S) AND ADDRESS(ES)

Air Force Office of Scientific Research
Bolling Air Force Base
Washington, DC 20332

10. SPONSORING/MONITORING AGENCY REPORT NUMBER

11. SUPPLEMENTARY NOTES

12a. DISTRIBUTION/AVAILABILITY STATEMENT

Unlimited

12b. DISTRIBUTION CODE

13. The crystal structure of fcc-based ordered Al_3Ti has been modified from the DO_{22}-type to the $L1_2$-type structure by the addition of 7.5 at.% Fe. This alloy is essentially single phase after homogenization at 1100°C at 100 h with a very small volume fraction of precipitates which have formed heterogeneously along dislocations. In the as-arc-cast condition, a high density of small precipitates occurred heterogeneously and homogeneously, in addition to the formation of a large sized, faulted second phase. In this case, precipitates which formed heterogeneously along dislocations are larger in size when compared to ones which formed in the homogenized condition. Precipitates which formed homogeneously in $L1_2$ grains were in the form of thin plates. Detailed crystal- and micro-structural observations of plate-shaped precipitates have revealed their precipitation on planes parallel to {001} $L1_2$. These precipitates have been determined to possess an ordered tetragonal structure which is composed of 6 fcc unit cells consisting of 4 titanium and 20 aluminum atoms. (SEE REVERSE)

14. SUBJECT TERMS

Dislocation cross slip, upper and lower yield points, ductile-to-brittle transition temperature, arc casting, homogenization heat treatment, four-point flexure, monotonic compression, $L1_2$ and DO_{22} crystal structures, second phases.

15. NUMBER OF PAGES

16. PRICE CODE

17. SECURITY CLASSIFICATION OF REPORT	18. SECURITY CLASSIFICATION OF THIS PAGE	19. SECURITY CLASSIFICATION OF ABSTRACT	20. LIMITATION OF ABSTRACT
Unclassified	Unclassified	Unclassified	None

In addition, the room temperature ductility of this $L1_2$-type Al_3Ti alloy has been improved substantially by hot isostatic pressing (HIP) after arc casting. This $L1_2$-type alloy can be deformed in compression to 11.4% at room temperature after HIPing, retaining the original shape of compressive specimens, while compressive specimens without HIPing fracture into small pieces when deformed to similar strain. Fracture occurs at room temperature by brittle transgranular cleavage with a smooth surface in HHTed specimens, while in HIPed specimens, fracture occurs by both transgranular and intergranular modes. Transgranularly fractured surfaces in the latter case have rough surfaces with fine structure, indicating ductile fracture as compared with that for HHTed specimens. In both HIPed and HHTed specimens, no fracture surfaces are flat and parallel to any crystallographic planes. High resolution electron microscopy has revealed that a pair of superlattice partial dislocations on a (111) plane have a spacing of approximately 11 nm (2-3 times larger than that for Al-23Ti-6Fe-5V), giving an antiphase boundary energy of 95 mJ/m^2. Since this energy is relatively low, the present alloy may be rendered ductile because of its ready emission of dislocations at crack tips, according to the Rice-Thomson criterion. Improvement of room-temperature ductility of this alloy is attributed primarily to the reduction of a large population of cavities which have formed upon arc casting.

R91-917992-2

Fatigue and Fracture of Intermetallic Alloys

ANNUAL REPORT

Contract F49620-89-C-0047

REPORTED BY: C. V. Cooper

H. R. P. Inoue

A. F. Giamei

L. H. Favrow

APPROVED BY: M. A. DeCrescente
Manager of Mfg. Tech.
and Process Research

DATE: 5/22/91

TABLE OF CONTENTS

1. INTRODUCTION

1.1 Overview

Future generations of aircraft gas turbine engines will, most likely, utilize hot-section materials based on systems other than the now-mature nickel-base superalloys. The identification of new systems has been motivated by the quest for higher combustion temperatures to satisfy the need for greater thrust-to-weight ratios and higher operating efficiencies. Among the potential systems is the broad class of materials known as intermetallics. Indeed, much research and development has gone into the study of intermetallic compounds based on the titanium-aluminum system, often with the focus on alloy development through ternary and quaternary additions as well as thermomechanical processing.

Three ordered compounds based on this binary system have been investigated to varying degrees: Ti_3Al (α_2:alpha-2), TiAl (γ:gamma), and Al_3Ti (η:eta). Because of the increasing tendency to form oxidation-protective alumina films and its inherently low density (3.3 g/cm^3), Al_3Ti has held particular attraction. As with the γ phase, a major difficulty with the η phase is inherent lack of ductility in the binary composition. Despite its intrinsic oxidation resistance, Al_3Ti, which in the binary form exhibits a DO_{22} (ordered tetragonal) crystal structure, has remained relatively understudied. The DO_{19} (α_2), the $L1_0$ (γ), the DO_{22} (η), and the well known $L1_2$ (τ) phases are all closed-packed and are related by variations in stacking and/or chemistry of the close-packed planes.

Through the addition of certain ternary transition metals, including iron, copper, or nickel, a phase transition from η to the ordered cubic, $L1_2$ can be induced. Being a crystal structure with higher symmetry over the DO_{22}, the $L1_2$ possesses potential advantages in mechanical behavior over the ordered tetragonal structure due to the increase in the number of active slip systems and the satisfaction of the well known Von Mises criterion for strain compatibility in polycrystals (Ref. 1).

Nonetheless, much research remains to be accomplished in the areas of understanding the exact mechanisms through which the $L1_2$ structure can be rendered increasingly ductile and the nature and location of the ductile-to-brittle transition phenomenon; furthermore, the entire areas of tensile and cyclic deformation remain virtually uninvestigated to date, at least in the open literature.

The attainment of the high symmetry, $L1_2$ structure is, of course, no guarantee that the alloy exhibits reasonable ductility. While the primary deformation mechanism in this structure, as discussed in greater detail below, is slip along octahedral planes, the cross slip of screw dislocations into cube planes creates sessile portions, which can lead to reduction in the tensile elongation to failure. High Peierls stresses may exist for certain dislocation dissociations, especially where fault energies are high (Refs. 2-8). Grain refinement, for example can lead to increases in flow stress, such that the cleavage stress is lower than the tensile yield stress. However, the cubic symmetry and close-packed nature of the $L1_2$ lattice offer the opportunity for useful ductility.

The intermetallic compounds of most interest show some solid solubility (*i.e.* they are not "line compounds") and are of high symmetry. The former condition pre-empts the possibility of forming small amounts of undesired equilibrium phases, while the latter condition maximizes the opportunities for multiple slip systems and the achievement of adequate low temperature fracture toughness. It turns out that the Al_3X compounds, where X is Ti or Nb, are DO_{22} compounds. This structure is closely related to $L1_2$, which is the crystal structure of the famous gamma prime phase. Even gamma prime has limited ductility under certain circumstances, but it is well understood and of great engineering significance. In addition, when Al_3Ti is alloyed with iron (or copper), the resultant $L1_2$ structure has a finite phase field width.

1.2 Review of the Literature

1.2.1 Phase Equilibria and Microstructural Studies

Because of the extreme lack of tensile ductility and fracture toughness at room temperature for Al_3Ti, most recent studies, as noted above, have focused on alloying additions to induce the transformation from DO_{22} to $L1_2$. The first to report this phase transformation were Raman and Schubert (Ref. 9), who accomplished the transition by dilute alloying additions of copper, nickel, or zinc in substitution for aluminum. Similar phase transformation have been noted more recently by Seibold (Ref. 10) through substitutions of iron for aluminum. While required concentrations of the selected ternary additions vary, the typical range lies from five to fifteen atomic percent.

Many recent studies have concentrated on the specific effects of alloying additions and rapid solidification processing on the resulting microstructures and phase fields. For example, Huang, Hall and Giogliotti (Ref. 11) investigated rapidly solidified Al-Ni-Ti in the atomic ratio of 65:10:25 and found predominantly but not exclusively cubic $L1_2$ phase. Powers, Wert, and Turner (Ref. 12) considered nickel-modified Al_3Ti, prepared by the non-consumable arc melting technique, in the atomic ratio of 67Al:8Ni:25Ti. Non-single-phase structures consisting predominantly of $L1_2$ were observed. Also, features exhibiting stacking-fault-like contrast were observed on {001} planes and were determined to be intrinsic stacking faults, which resulted from the dissociation of a_o<110>{001} dislocations. These faults were determined to be sessile in nature and did not participate in the deformation process.

Tarnacki and Kim (Ref. 13) have examined arc-melted and rapidly solidified τ phase which had been modified by copper additions leading to Al_5CuTi_2, or by small amounts of boron or manganese. Rapid solidification by melt-spinning was found to refine the microstructure significantly and increase the microhardness slightly compared to the as-cast alloy. The as-cast microstructure of the copper ternary was two-phase, with the primary phase described as having the "nominal composition" and the dispersed second phase being globules with sizes ranging from 3-20 μm. X-ray diffraction

analysis verified the $L1_2$ crystal structure for both the as-cast and rapidly solidified forms. In addition, fine, second-phase particles on the order of 100 nm which were Cu-rich were resolved by TEM. While mechanical property determinations were not the focus of Tarnacki and Kim's study, the addition of copper and the achievement of the $L1_2$ were observed to result in no improvements in ductility over the binary Al_3Ti.

Mazdiyasni *et al.* (Ref. 14) examined the phase equilibria of iron, nickel, and copper-modified Al_3Ti prepared by vacuum arc melting. The resulting phase-field width was determined using x ray diffraction of powder samples following homogenization and quenching from 800 and 1200°C. Single-phase τ was found for all three ternary systems for the 1200°C isotherm. At 800°C, the width of the single-phase field was reduced for the iron and nickel ternary systems; the phase boundary was not determinable for the nickel ternary due to the nucleation of a fine, second-phase precipitate. These authors found that the $L1_2$ phase was stable to at least 1200°C in all three alloy systems.

However, Tarnacki and Kim (Ref. 15) failed to produce single-phase τ in the Al-Ni-Ti ternary system despite a post-arc-melting homogenization heat treatment for 96 hr at 1100°C in the $Al_{67}Ni_8Ti_{25}$ ternary system.

A very exciting result from this laboratory (UTRC) is the achievement of phase-pure τ in the iron ternary system. As is to be discussed further in section 3.0, single phase $L1_2$ with only isolated carbides, believed to be the result of impurities introduced with the iron, has been produced recently by the hot-pressing of prealloyed, ball-mill-attrited powders. This has been achieved despite the well known difficulties associated with establishing equilibrium in peritectic systems.

To date, little information is available on the DO_{22} system, Al_3Nb. While the likelihood of transforming this system to phase-pure $L1_2$ remains unclear, unpublished reports indicate that additions of chromium, yttrium, and tungsten lead to a stable, oxidation-resistant, fracture-tough alloy. Furthermore, it should be possible to transform iron- and titanium-modified Al_3Nb to the $L1_2$ crystal structure through alloying, by analogy to Al_3Ti.

1.2.2 Deformation Studies

By comparison to the published literature dealing with microstructural and phase equilibria aspects, that which focuses on the deformation behavior of tau phase is rather scant. Recent studies of the deformation behavior of binary Al_3Ti (DO_{22}) have been undertaken by Tamaguchi *et al.* (Refs. 16,17). These authors have reported that the predominant deformation mode is that of deformation twinning on the (111) [112] system, which retains the DO_{22} lattice symmetry. At elevated temperatures, some evidence for deformation through slip in addition to twinning was noted by Burgers vector analysis; however, binary Al_3Ti has proven to be very brittle in tension at room temperature.

Deformation research in the iron-based $L1_2$ system has been conducted by Kumar and Pickens (Ref. 18) on ternary and quaternary-modified $Al_{22}Fe_3Ti_8$. Their study endeavored to promote a comparative understanding of the compressive behavior of τ phase based on the ternary and a 2 at.% vanadium (in substitution for titanium) quaternary alloy and to establish the temperature dependence of the compressive flow stress. The major finding of their research was a substantial decrease in the magnitude of the positive dependence in the flow stress with temperature along with a second peak in the vanadium quaternary compared to the ternary alloy.

An investigation of the mechanical properties of a nickel-ternary τ alloy, including compressive stress-strain and fracture toughness based on bend tests, was the focus of a recent paper by Turner, Powers, and Wert (Ref. 19). These authors reported substantial plasticity in compression ($\varepsilon_f \cong 14\%$) and a fracture toughness of 3 $MPa \cdot m^{1/2}$. Interestingly, the bend specimen fracture surfaces displayed major cleavage facet poles within a few degrees of [001], [110], [111], [112], and [113], which suggested that the alloy can fail on virtually any plane, the orientation of which is nearly perpendicular to the tensile axis. The lack of tensile ductility was explained by these researchers on the basis of the Rice-Thompson model (Ref. 20), in which dislocation emission from a crack tip inhibits or prevents plastic crack tip blunting as suggested by the Gb/Γ ratio being greater than 10, where G is the shear modulus, **b** is the Burgers vector and Γ ("gamma") is the surface free energy.

Porosity and the presence of a more brittle second phase are additional problems which complicate the measurement of the tensile properties of the τ phase. For example, Turner, Powers, and Wert (Ref. 19) report that, while the porosity of the as-cast alloys is quite low, the long-term, high-temperature homogenization heat treatment causes appreciable increases in porosity.

2. EXPERIMENTAL PROCEDURES

2.1 Alloy Casting

Intermetallic alloys for use in this program were prepared by arc melting using starting materials of two initial purities: (1) commercial purity and (2) high purity. In the latter of the two, close attention was paid to the elimination of impurities from the initial constituents which were believed to be deleterious to the cast ingots either during their cooling or during the subsequent determination of its properties. The chemical compositions of the starting constituents for the higher purity alloys were previously reported. For both purities of starting materials, ingots were produced with a composition, in atomic percent, of 67.5% Al, 25% Ti, and 7.5% Fe. Arc casting was accomplished using a specially constructed, tri-electrode apparatus which was designed to accommodate batch-size maxima of between 150 and 250 g, depending on constituent and alloy density. Purified argon gas, gettered by flowing standard bottled gas over hot Ti chips, was used to create a protective atmosphere for the melting and solidification processes. As a measure to reduce nitrogen and oxygen impurity levels further, a titanium bar was melted in the chamber prior to melting the alloy constituents. Typical effluent impurity levels in the argon gas, monitored throughout the melting and casting procedures, were on the order of 10^{-6} ppm by weight (one part impurity in 10^{12} parts argon).

Buttons were cast in hemispherical, water-cooled copper hearths using a minimum of three melting and resolidification sequences; to minimize macrosegregation, the cast buttons were "flipped" between melting operations. In addition to the button configuration, drop castings of an iron alloy by means of a small orifice in the copper hearth were attempted as preliminary trials to the rapid solidification of the Fe-modified Al_3Ti alloy using a dual-wheel ribbon maker. This process was being assessed as an approach to the production of ultra-clean ribbon to be comminuted subsequently into powder.

To facilitate the production of four-point flexure and monotonic compression specimens, ingots which were cast using the hemispherical hearth were secondarily cast in a flat-bottom hearth using procedures similar to those described above for the hemispherical hearth to produce plate castings.

2.2 Specimen Preparation and Heat Treatment

To date, specimens of two geometries have been produced for study; both geometries have been produced from castings as well as compacted powders. The first of these is a thin beam, from which four-point flexure experiments have been conducted as a function of ambient temperature. The second of the specimen geometries is that of a right circular cylinder, from which monotonic, quasi-static compressive properties have been determined. For both geometries, high-purity buttons and plates were wire electro-discharge machined (EDM) in several heat-treated conditions. A determination of the mechanical properties of the lower purity castings was rendered impossible due to their spontaneous fracture following solidification during cooling to room temperature.

In addition to the as-cast (AC) condition, monotonic compression and flexure properties were determined from specimens in the homogenization-heat-treated (HHT) condition. The homogenization heat treatment consisted of heating the machined specimens to 1100°C for 100 h in a controlled atmosphere furnace using argon gas which was purified in the same manner and to the same degree as described above for the casting process.

Following arc casting, some ingots were given a third treatment, that of hot isostatic pressing (HIP), to reduce the level of porosity compared to the as-cast condition. This process consisted of wrapping the ingots with Ta foil, placing the wrapped ingots in a stainless steel (SS) enclosure, evacuating, crimping, and sealing the SS container, placing the enclosed ingot in the pressure vessel, supplying an overpressure of argon to 1200 psig at ≅ 25°C, increasing pressure to 1200 psi at constant temperature, elevating temperature at 30°C/min and pressure at 1000 psi/min to 1100°C and 25,000 psi, respectively, and holding at temperature and pressure for 4 h.

A final processing treatment consisted of hot pressing (HP) comminuted powders in titanium-zirconiun molybdenum (TZM) dies with aluminum oxide inserts to a pressure of 5000 psi at a temperature of 1100°C for 4 h.

Comminution of cast buttons from both the high purity and the nominal purity starting materials was accomplished using a standard ball mill with stainless steel comminutors, following which the alloy powders were graded with standard metal sieves. Ball milling and subsequent grading of powders were accomplished both in a protective atmosphere and in laboratory air, the former making use of an air-tight glove box following evacuation and a thorough purge with flowing argon. Powder which remained +325 mesh following comminution, that is, that which failed to pass through the 325 mesh sieve, was recycled through the ball milling and sieving processes. In order to determine the effects of powder size on the density and microstructure of hot pressings, powder which was sieved to -400 mesh was produced, hot pressed, and examined as well.

2.3 Microscopy

Optical (OM), scanning electron (SEM), and transmission electron microscopies (TEM) and selected area electron diffraction (SAED) have been applied in complementary fashion to characterize the microstructures of the Fe-modified Al_3Ti alloy in the AC and HHT conditions. To capitalize on mutual interests common to researchers at UTRC and the University of Illinois, UTRC has supplied undeformed and compressively deformed specimens to Professor H. R. P. Inoue of the Department of Materials Science and Engineering for TEM and electron diffraction analyses. Undeformed (virgin) and monotonically compressed cylindrical specimens were sectioned for TEM into discs having dimensions of 1 mm thickness and 4 mm diameter. The sectioning plane was perpendicular to the compressive axis, the axis of rotational symmetry for the cylinders, again accomplished using wire EDM. Discs for TEM were mechanically polished and subsequently electropolished to electron transparency using a twin-jet polisher. TEM and SAED were conducted using a Hitachi H-800 microscope operated at 200 keV.

2.4 Mechanical Behavior

As noted above, the mechanical properties of AC and HHT materials were determined by monotonic four-point flexure and compression experiments. Both configurations made use of a servo-hydraulic testing machine, the temperature range for testing was from 22 to 1100°C, and the strain rate was 3.5×10^{-4}/s. All flexure and compression experiments were accomplished in an atmosphere of purified argon.

3. RESULTS AND DISCUSSION

3.1 Microscopic Observations and Crystallographic Orientation of Second Phase Precipitates

3.1.1 Microstructures

Optical microscope observations showed that as arc-cast samples consist of a two-phase microstructure containing an $L1_2$ phase and a second phase, as shown in Fig. 1. This second phase has planar faults which may be twins which have formed in order to accommodate interfacial strain with the $L1_2$ matrix, as shown in Fig. 2. After homogenization, this second phase almost completely disappears; that is, the present alloy becomes essentially single phase with an $L1_2$ structure. Transmission electron microscope observations of homogenized specimens, however, revealed tiny precipitates on dislocation segments, as shown in Fig. 3. Although it is not yet clear whether these tiny precipitates are the residues of the second phase, they may play a significant role in providing good mechanical properties at high temperature. Since these precipitates are small in size and in quantity, in the present work, characterization has been performed on fine plate-shaped precipitates present in abundance in as-arc-cast specimens.

Two types of fine precipitates have been observed in as arc-cast specimens. Typical examples are shown in Figs. 4 and 5. Figure 4 shows fine band-shaped precipitates which have formed heterogeneously along grown-in and thermal-stress-induced dislocations, while Fig. 5 shows fine plate-shaped precipitates having formed homogeneously in grains of the $L1_2$ matrix. Such heterogeneous precipitates are about 20 nm thick and show fringes with a fringe thickness of about 2-3 nm. These precipitates are considered to be similar to those observed in homogenized specimens, as shown in Fig. 3.

Microstructural observations have revealed that plate-shaped precipitates occur homogeneously parallel to {001} planes of $L1_2$ matrix. In Fig. 5, plate-shaped precipitates are clearly seen to have formed parallel to (100)

planes. The diffraction pattern taken from the area of this micrograph shows evident streaks, corresponding to precipitates parallel to (100) planes. Careful observation of this figure reveals that there are also precipitates which are parallel to (010) and (001) planes. The presence of precipitates which have formed on three sets of {001} planes is seen clearly in Fig. 6.

3.1.2 Crystal structure of plate-shaped precipitates

The crystal structure of plate-shaped precipitates which have formed on {001} planes was determined using electron diffraction patterns taken from arc-cast specimens. It was noticed that when the direction of the incident electron beam was parallel to zone axes of the matrix having low Miller indices, no extra diffraction spots were observed except streaks, which pass through diffraction spots of the $L1_2$ matrix and are perpendicular to {001} planes of the matrix. They are, for example, [011], [111], and [121], as shown in Fig. 7(a,b,c). Conversely, many extra spots appeared in the case when the incident electron beam was parallel to zone axes having high Miller indices, as shown in Fig. 7(d,e,f). These extra spots cannot be indexed by assuming DO_{22} and DO_{23} structures, all of which are $L1_2$-based structures, as shown in Fig. 8(b,d). Taking into consideration that some extra spots appear at positions h/3, k/3, l/3 and 2h/3, 2k/3, 2l/3, where h, k and l are Miller indices of the $L1_2$ matrix, another $L1_2$-based structure was assumed, which is composed of three $L1_2$ unit cells, as shown in Fig. 8(c). However, this structure also cannot explain most of the extra spots observed.

A new ordered tetragonal structure proposed for the observed plate-shaped precipitates is shown in Fig. 9. The unit cell of this tetragonal structure is composed of six fcc unit cells containing 4 titanium atoms and 20 aluminum atoms. It should be noted that this structure is aluminum rich compared with the $L1_2$-based structures shown in Fig. 8. The atomic ratio (Al:Ti) of this proposed structure is 5:1, which is compared to a ratio of 3:1 for all the structures shown in Fig. 8. Although iron atoms are not shown in Fig. 9, they are considered to locate randomly at aluminum sites. Assuming this ordered tetragonal structure, all the diffraction patterns shown in Fig. 7 can be indexed.

In order to index the diffraction patterns shown in Fig. 7, the following lattice parameters are used:

$a_{ppt} = a_{\tau} = 0.394$ nm, and
$c_{ppt} = 6 \times a_{\tau} = 2.364$ nm,

where τ is the phase having $L1_2$ crystal structure.

In addition, the following consideration is also needed. From the observations of the habit planes of the plate-shaped precipitates, there are six possible orientation relationships between this precipitate phase and the $L1_2$ matrix phase, suggesting the presence of six variants. However, due to equivalency, the total number of variants reduces to three. These three variants must be taken into account in indexing diffraction patterns taken from arc-cast specimens. The orientation relationships for these variants are as follows:

variant 1: **a** [100] ppt // **a** [100] $L1_2$
b [010] ppt // **b** [010] $L1_2$
c [001] ppt // **c** [001] $L1_2$,

variant 2: **b** [010] ppt // **a** [100] $L1_2$
c [001] ppt // **b** [010] $L1_2$
a [100] ppt // **c** [001] $L1_2$,

variant 3: **c** [001] ppt // **a** [100] $L1_2$
a [100] ppt // **b** [010] $L1_2$
b [010] ppt // **c** [001] $L1_2$.

Under the assumption of this proposed structure and these three orientation relationships, all extra spots can be indexed, as shown in Fig. 7(d,e,f).

3.2 Comparison of Fracture Properties between HIP and HHT Conditions

3.2.1 Microstructures

Previous optical microscope observations (Ref. 25) have revealed blocky second-phase precipitates in as-cast specimens. In addition, it has also been observed by transmission electron microscopy that there are both fine platelets (10 nm wide) forming homogeneously along {001} planes and band-shaped precipitates forming heterogeneously along dislocations. After HIPing, such blocky precipitates disappear. In their place, structures with a dendritic morphology appear in the form of crosses, which seem to have some specific orientation relationship with the $L1_2$ matrix, as shown in Fig. 10. These could be phantom dendrites, a residual dendritic pattern which appears after precipitates nucleate and grow in the dendrite cores. After homogenization annealing, conversely, the alloy becomes essentially single phase with a very small volume fraction of precipitates having nucleated along dislocations (Ref. 23). As will be shown below, room-temperature ductility is improved by HIPing. Hence, it is of great importance to identify microstructures of HIPed specimens and to determine the relationship between these microstructures and fracture properties. Such a study is currently in progress.

3.2.2 Temperature dependence of yield stress and ductility

Both HHTed and HIPed specimens were deformed in compression at various temperatures. Yield stress values obtained were plotted as a function of test temperature. No anomalous temperature dependence of the yield stress has been obtained, which is a common and important property of many nickel-based $L1_2$-type compounds such as Ni_3Al and Ni_3Ge. As shown in Fig. 11, the yield stress decreases slightly from room temperature to 400°C, remaining almost constant through 750°C, and then decreasing again at higher temperatures. Similar temperature dependence has been observed also in Pt_3Al having the same $L1_2$ structure (Ref. 26). The absence of an anomalous

temperature dependence of yield stress in the present alloy is rather interesting because transmission electron microscope observations have revealed that screw dislocations cross slip from {111} to {001} planes in the alloy when deformed at 1100°C (Ref. 23). Among many nickel-based $L1_2$-type compounds, such cross slipping is known to be the primary origin of the anomalous temperature dependence of the yield stress (Ref. 27).

Figure 11 also shows plastic strain obtained in the compression experiments. Compared with DO_{22}-type Al_3Ti, the modified $L1_2$-type Al_3Ti alloy shows improvement in room-temperature ductility. Furthermore, as will be shown below in Fig. 12, room-temperature ductility is substantially improved after HIPing, although the apparent plastic strain (approximately 11%) obtained is almost the same for both HIPed and HHTed specimens. At temperatures higher than 400°C, both HHTed and HIPed specimens can be deformed to more than 12%. The proposed explanation for this behavior is that uniaxial compression tends to close existing pores and voids, reducing their contribution to the fracture event.

3.2.3 Fracture morphologies

Figure 12 shows a portion of both HIPed and HHTed specimens deformed in compression at room temperature. Clearly evident is the brittle nature of the HHT condition. Specimens fracture into small pieces, and no original shape is retained, as shown in Fig. 12 (a). Conversely, HIPed specimens retain their original shape even following the application of considerable plastic deformation (a strain of 11%). These specimens fracture by a few large vertical cracks propagating from top to bottom, as shown in Fig. 12(b).

High magnification scanning electron micrographs taken from the specimens in Fig. 12 reveal clear contrast of microstructural features. Figure 13(a) is a micrograph taken from region A of Fig. 12(a), where comparably large pieces are present, showing a high density of cavities. Fracture in this case occurs by brittle transgranular cleavage, which probably initiates at cavities

formed upon solidification, Fig. 13(b). As seen in this figure, fracture surfaces are relatively smooth but not parallel to any crystallographic planes with low Miller indices. Essentially similar structures are obtained from region B of Fig. 12(a), where the specimen Fig. 12(a) becomes fragmented upon fracture. Compared to fracture surfaces for HHTed specimens, however, fracture surfaces are rather rough and irregular in the case of HIPed specimens, Fig. 13(c). In addition, both intergranular and transgranular fractures occur, as shown in Fig. 13(d). It should be noted that cavities are reduced significantly with retention of a small density of cavities after HIPing, as shown in Fig. 13(d). Intergranular fracture in this case has probably occurred due to strengthening against transgranular fracture through the reduction in the size and density of cavities. Fracture surfaces of HIPed and HHTed specimens are also observed after deformation in compression at 400, 750, and 1100°C. In both cases, no significant change in fracture morphologies has been observed by increasing the test temperature, but it appears that fracture surfaces become more irregular and rugged with increasing temperature.

3.2.4 Dislocation structure

The structure of dislocations introduced in HHT specimens by deformation in compression at room temperature has been investigated by means of HREM. Figure 14 is a micrograph taken from a thin foil parallel to the (001) plane, showing a pair of superlattice partial dislocations with a Burgers vector of a/2[101] on a (111) plane. In the micrograph, the imaging atoms are considered to be titanium atoms located at the corner sites of the $L1_2$ unit cells. Taking the lattice parameter of the alloy as 0.395 nm and the angle between the (001) and (111) planes into consideration, a spacing of 11 nm between the paired superlattice dislocations is obtained. It is obvious in this case that these dislocations do not lie on any {001} planes but lie on the (111) plane.

The APB energies, γ_{APB}, can be calculated using the equation for screw dislocations,

$$\gamma_{APB} = G\, b^2/2\pi\, r,$$

where G is the shear modulus, b the Burgers vector and r the spacing between two screw dislocations. Using a value for G of 84 GPa (Ref. 25), a Burgers vector for 1/2[101] of 0.279 nm, and the measured superpartial separation of 11 nm, the APB energy is calculated to be 95 mJ/m^2. This value is much lower than those reported for Al_3Sc (313 mJ/m^2) (Ref. 22) and Al-23Ti-6Fe-5V (274 mJ/m^2) (Ref 22). According to the Rice-Thomson criterion (Ref. 20), dislocations are considered to be emitted readily at or near crack tips for the present alloy due to the large separation between the two superpartial dislocations. This suggests that the alloy is intrinsically relatively ductile; hence it should be possible to improve the ductility of this alloy through the complete elimination of porosity.

4. SUMMARY AND CONCLUSIONS

The crystal structure of the stoichiometric Al_3Ti intermetallic compound can be modified from the DO_{22} to the $L1_2$ structure by adding 7.5 at.% Fe to substitute for a portion of aluminum. This alloy is essentially single phase after homogenization at 1100°C for 100 h with a very small volume fraction of precipitates having formed along dislocations. Conversely, in the case of the as-cast condition, the alloy contains band-like precipitates which have formed along dislocations and a high density of very thin, plate-shaped precipitates which are parallel to {001} planes of the $L1_2$ matrix. The crystal structure of these plate-shaped precipitates is proposed to be an ordered tetragonal structure consisting of six fcc unit cells stacked along the "c" axis. This proposed structure contains 4 titanium atoms and 20 aluminum atoms with iron atoms in substitution for aluminum atoms. All diffraction patterns obtained were indexed by assuming this structure and two or three variants of the precipitate phase. Since there is a possibility that titanium atoms can be located at positions other than those proposed, detailed intensity calculations of diffraction patterns or high resolution electron microscopy may be needed to determine atom positions accurately.

In addition, the room temperature ductility of an $L1_2$-type Al_3Ti alloy containing 7.5 at.% Fe has shown little improvement following hot isostatic pressing (HIP) after arc casting. However, fracture occurs at room temperature by brittle transgranular cleavage with a smooth surface in HHTed specimens, while in HIPed specimens, fracture occurs by both transgranular and intergranular modes. Transgranularly fractured surfaces in the latter case have rough surfaces with fine structure, indicating ductile fracture, in contrast to the behavior and fracture morphology of HHTed specimens. In both HIPed and HHTed specimens, no fracture surfaces are flat and parallel to any crystallographic planes. High resolution electron microscopy has revealed that a pair of superlattice partial dislocations on a (111) plane have a spacing of approximately 11 nm (2-3 times larger than that for Al-23Ti-6Fe-5V) giving an antiphase boundary energy of 95 mJ/m^2. Since this energy is relatively low, the

present alloy may be ductile because of its ready emission of dislocations at crack tips, according to the Rice-Thomson criterion. Improvement in the room-temperature ductility of this alloy is attributed primarily to the reduction of a large population of cavities which have formed upon arc casting.

5. WORK IN PROGRESS

Current efforts are being concentrated in several parallel areas, as noted below.

5.1 Tensile and Fatigue Data

In order to determine the influence of powder particle size on tensile and fatigue properties, a fixture has been devised, as shown in Figure 15. This fixture utilizes counter-rotating cams to grip "dogbone" shaped specimens, machined so as to closely approximate the cam profiles of the fixture. The cams rotate through radii of curvature profiles machined on specimen contact surfaces as well as the reverse side of the specimen contacting cams. This fixture allows for line loading of specimens in the radii and blend areas. In addition, as all four radii are loaded, this configuration produces specimen self-alignment. The fixture has been fabricated out of TZM for elevated temperature testing.

5.2 The Effects of Powder Size

A determination of the microstructure and properties of hot pressed powder which has been comminuted and graded to -325 or -400 mesh from two purities of starting materials is in progress. The major objective of this segment of the study is to determine the influence of powder particle size on the microstructure and properties of the 7.5 at.% Fe alloyed with Al_3Ti. Should the density and properties of plates which have been hot pressed from -325 mesh powder be equivalent or nearly equivalent to those of the -400 mesh product, -325 mesh powder will be selected for use because of the increased yield and decreased intensity of labor required for its production.

5.3 The Effects of Iron Content

To resolve the interesting microstructure noted in the cast and HIPed alloy containing 7.5 at.% Fe, namely the presence of an interdendritic second phase, master alloys containing 6.5 and 8.5 at.% Fe have been cast and are being examined in several conditions, including as-cast, cast plus HHT, cast plus HIP, and cast plus HIP plus HHT. The third of these treatments, the cast plus HIP plus HHT, is being given to the 7.5 at.% alloy, as well, to determine if the dendritic second phase is a non-equilibrium structure.

5.4 Niobium Alloy Studies

Efforts are currently in progress to produce additional alloy compositions, in which Nb is added in substitution for Ti and the Al and Fe contents remain constant at 67.5 and 7.5 at.%, respectively. As with the ternary compositions, arc-cast ingots from these quaternary compositions ar to be produced, comminuted, and consolidated using hot pressing and/or hot isostatic pressing to produce plates, from which specimens to determine mechanical properties are to be fabricated. For all alloy compositions, a major emphasis of the third and final year of the contract is the determination of the fracture and fatigue properties, as well as optimal fabrication procedures, for the several alloy compositions identified.

6. REFERENCES

1. R. Von Mises, Z. Ang. Math. Mech., 8, 161 (1928).

2. S.M. Copley, B.H. Kear and G.M. Rowe, Mater. Sci. Eng., 10, 87 (1972).

3. B.H. Kear, A.F. Giamei, J.M. Silcock and R.K. Ham, Scripta Metall., 2, 287 (1968).

4. B.H. Kear, A.F. Giamei, G.R. Leverant and J.M. Oblak, Scripta Metall., 3, 455 (1969).

5. B.H. Kear, J.M. Oblak and A.F. Giamei, *Proc. Second Int'l Conf. on Strength of Metals and Alloys*, 1155 (1970).

6. B.H. Kear, J.M. Oblak and A.F. Giamei, Metall. Trans., 1, 2477 (1970).

7. B.H. Kear, A.F. Giamei and J.M. Oblak, Scripta Metall., 4, 567 (1970).

8. J.E. Dcherty, A.F. Giamei and B.H. Kear, Metall. Trans. A, 6A, 2195 (1975).

9. A. Raman and K. Schubert, Z. Metallkd., 56, 99 (1965).

10. A. Seibold, Z. Metallkd., 72, 712 (1981).

11. S.C. Huang, E.L. Hall and M.F.X. Gigliotti, J. Mater. Res., 3, 1 (1988).

12. W.O. Powers, J.A. Wert and C.D. Turner, Philos. Mag. A., 60, 227 (1989).

13. J. Tarnacki and Y.W. Kim, Scripta Metall., 22, 329 (1988).

14. S. Mazdiyasni, D.B. Miracle, D.M. Dimiduk, M.G. Mendiratta and P.R. Subramanian, Scripta Metall., 23, 327 (1989).

15. J. Tarnacki and Y.-W. Kim, in *Dispersion Strengthened Aluminum Alloys*, Editors Y.W. Kim and W.M. Griffith, Warrendale, PA: The Metallurgical Society, 741 (1988).

16. M. Yamaguchi, Y. Umakoshi and T. Yamane, Philos. Mag. A, 55, 301 (1987).

17. M. Yamaguchi, Y. Umakoshi and T. Yamane, in *High Temperature Ordered Intermetallic Alloys II*, Editors N.S. Stoloff, C.C. Koch, C.T. Liu and O. Izumi, Pittsburgh: Materials Research Society, 207 (1987).

18. K.S. Kumar and J.R. Pickens, Scripta Metall., 22, 1015 (1988).

19. C.D. Turner, W.O. Powers and J.A. Wert, Acta Metall., 37, 2635 (1989).

20. J.R. Rice and R. Thompson, Philos. Mag., 29, 73 (1974).

21. S. Zhang, J. P. Nic, and D. E. Mikkola, Scripta Metall., 24, 57 (1990).

22. E. P. George, W. D. Porter, H. M. Henson, W. C. Oliver, and B. F. Oliver, J. Mater. Res. 4, 78 (1989).

23. H. R. Pak, C. M. Wayman, L. H. Favrow, C. V. Cooper, and J. S. L. Pak, Mat. Res. Soc. Symp. Proc. (1990), in press.

24. W. D. Porter, K. Hisatsune, C. J. Sparks, W. C. Oliver and A. Dhere, Mat. Res. Soc. Symp. Proc. 133, 657 (1989).

25. E. P. George, J. A Horton, W. D. Porter, and J. H. Schneibel, J. Mater. Res. 5 1639 (1990).

26. D. M. Wee, O. Noguchi, Y. Oya. and T. Suzuki, Trans. Jpn. Inst. Met. 21 237 (1980).

27. H.-R. Pak, T. Saburi, and S. Nenno, Trans. Jpn. Inst. Met. 18 617 (1977).

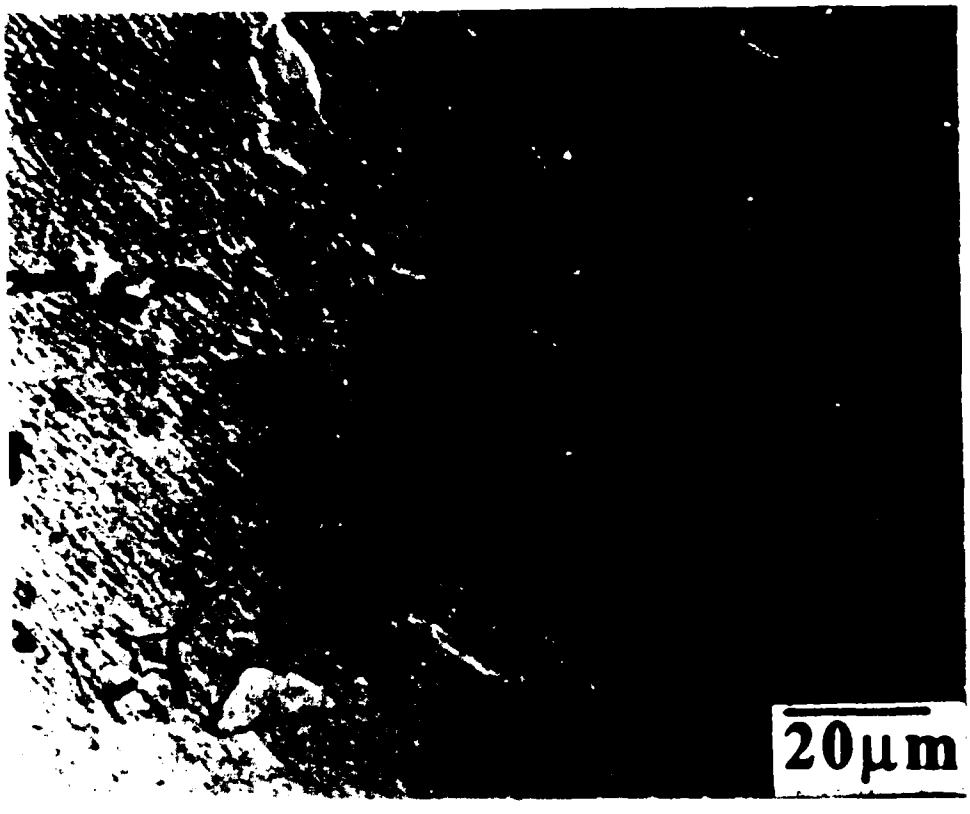

Figure 1 Optical micrograph of an as-arc-cast $Al_{67.5}Ti_{25}Fe_{7.5}$ alloy, showing at least two phases.

Figure 2 Transmission electron micrograph of as-arc-cast $Al_{65}Ti_{25}Fe_{10}$ alloy, showing a large faulted precipitate.

Figure 3 Dark field micrograph of a homogenized $Al_{67.5}Ti_{25}Fe_{7.5}$ specimen, showing tiny precipitates on dislocations. A 111 $L1_2$ reflection has been used.

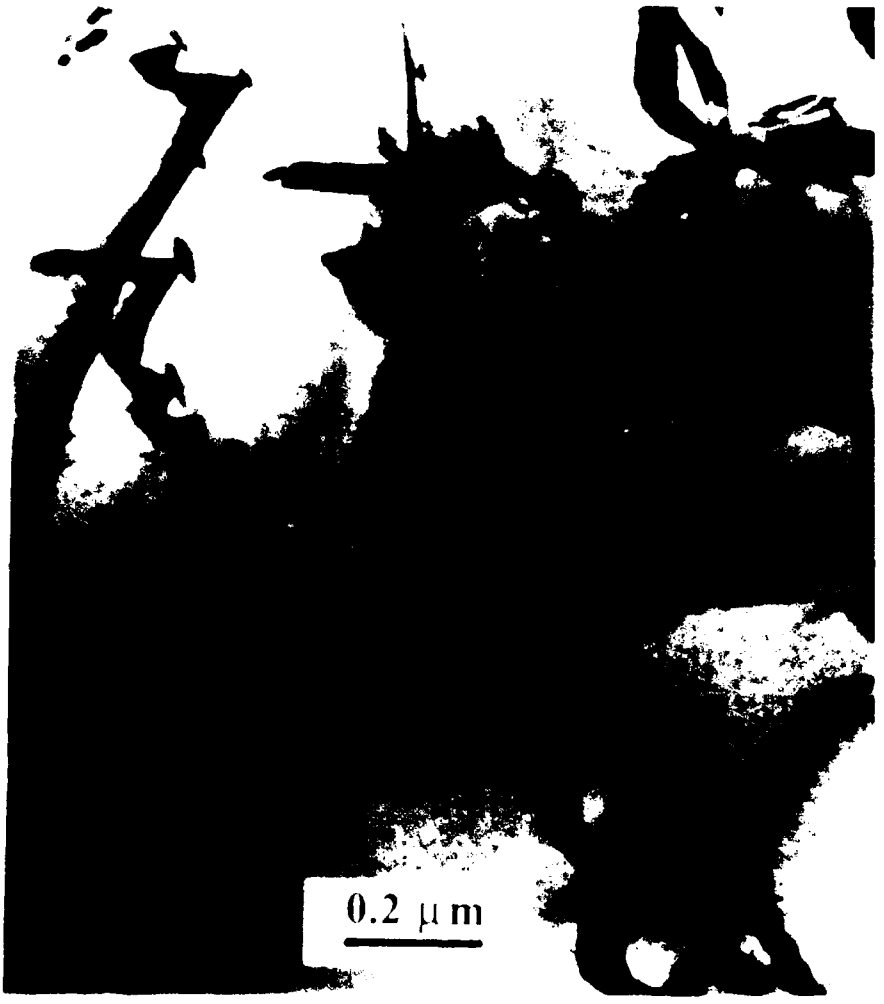

Figure 4 Heterogeneous precipitates along dislocation in an as-arc-cast $Al_{67.5}Ti_{25}Fe_{7.5}$ specimen.

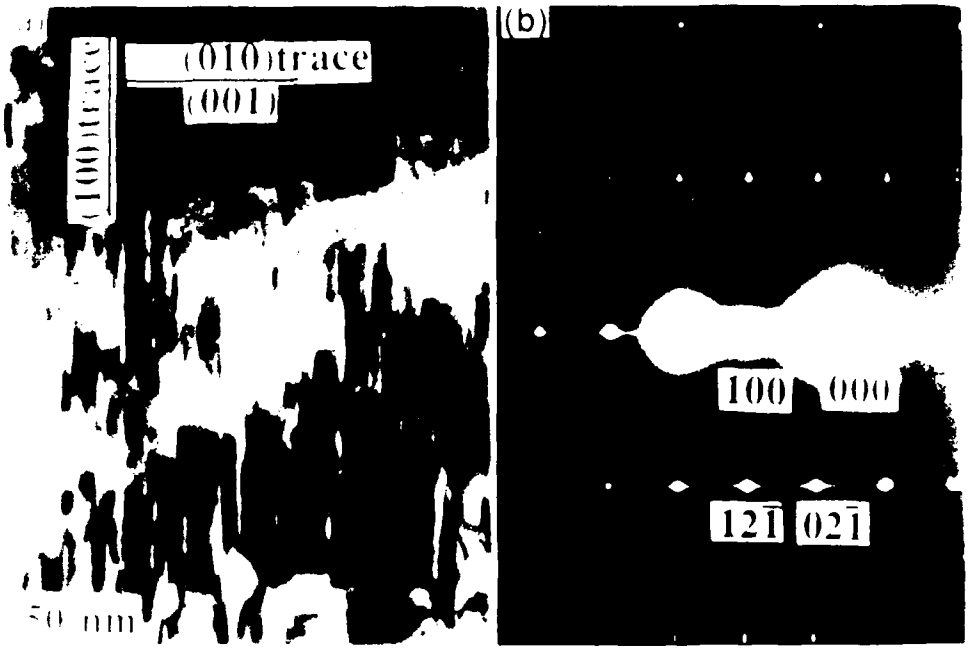

Figure 5 Plate-shaped precipitates in $L1_2$ grains of an as-arc-cast specimen (a) dark field image of an ordered 100 reflection, and (b) [012] zone axis of the $L1_2$ matrix.

Figure 6 Plate-shaped precipitates on three sets of {001} planes of the $L1_2$ matrix in an as-arc-cast specimen. Foil plane nearly parallel to (615).

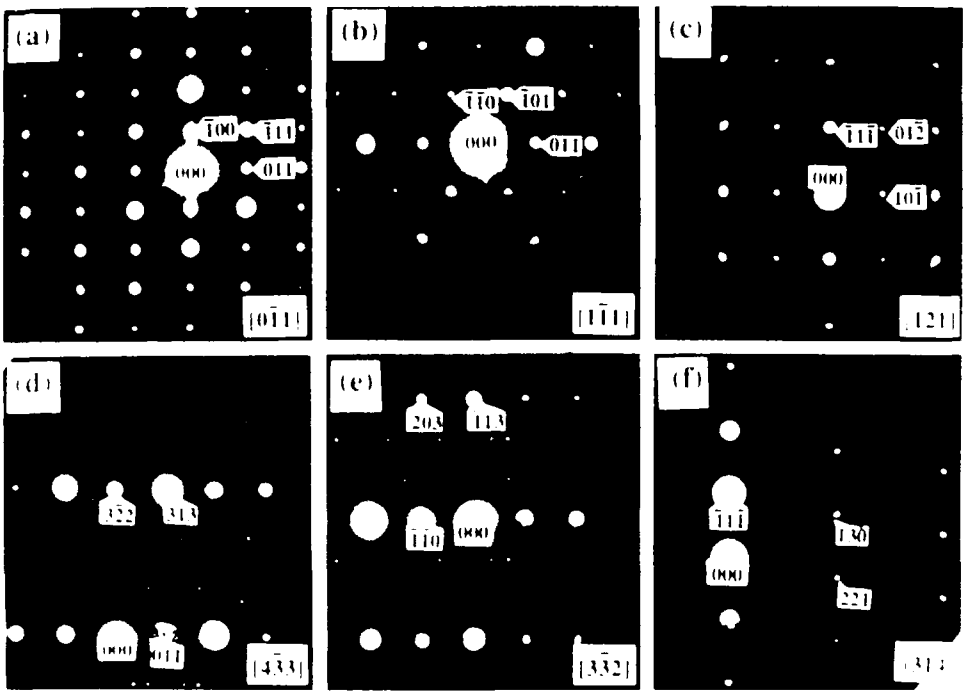

Figure 7 Electron diffraction patterns taken from as-arc-cast $Al_{67.5}Ti_{25}Fe_{7.5}$ specimens. Zone axes indexed by $L1_2$: (a) [011], (b) [111], (c) [121], (d) [433], (e) [332] and (f) [314].

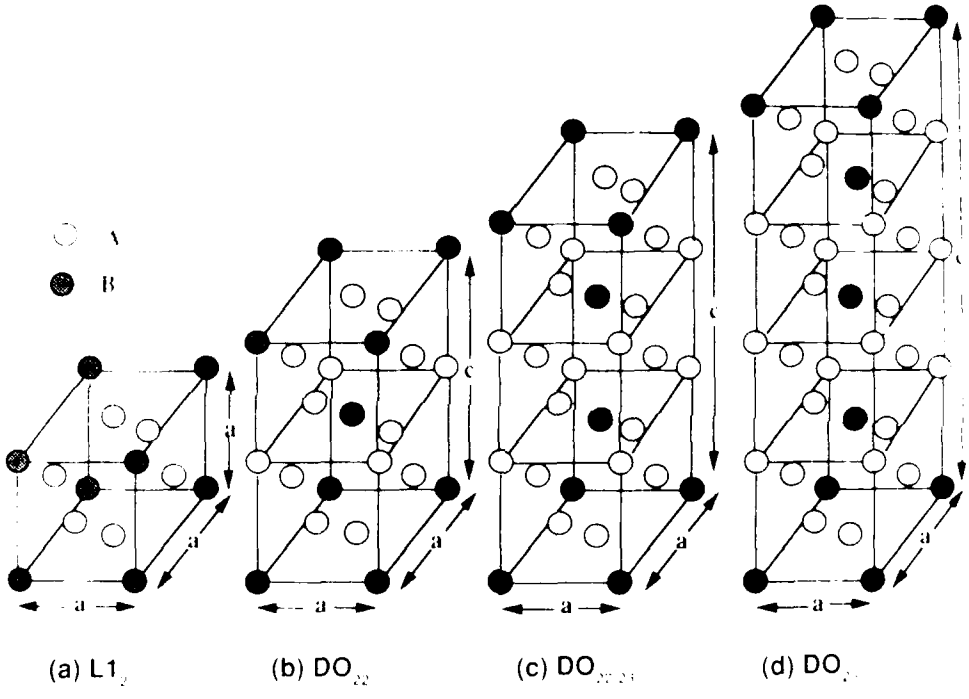

Figure 8 Unit cells of L1-based structures. (a) L1, (b) DO, (c) DO, and (d) DO.

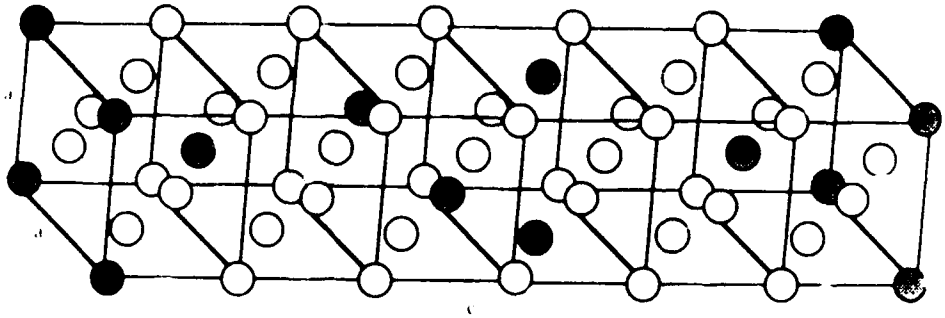

Figure 9 A proposed ordered tetragonal structure consisting of six fcc unit cells

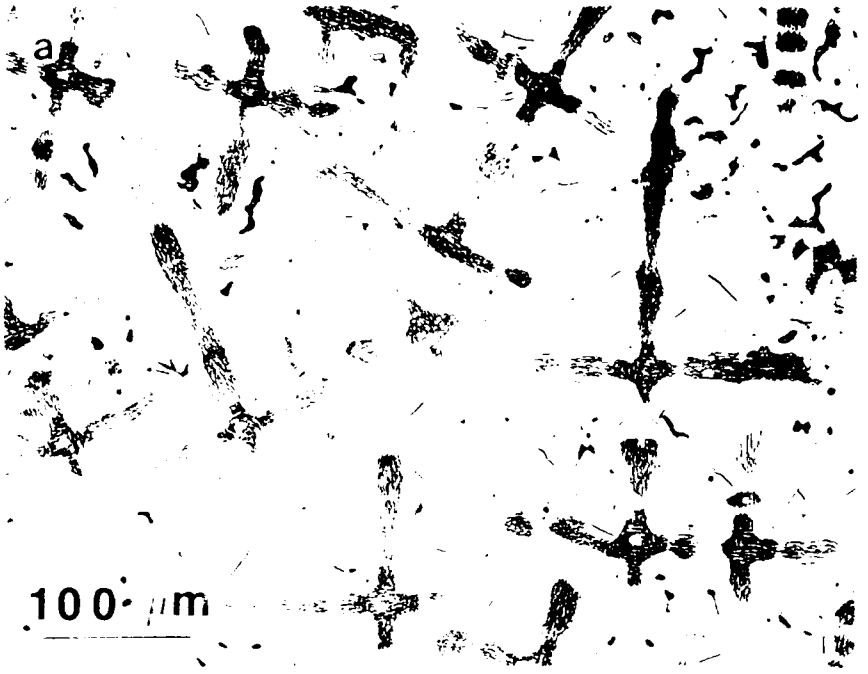

Figure 10. Optical micrographs showing a dendritic structure appearing in HIPed specimens after a) casting (a) low magnification (b) high magnification

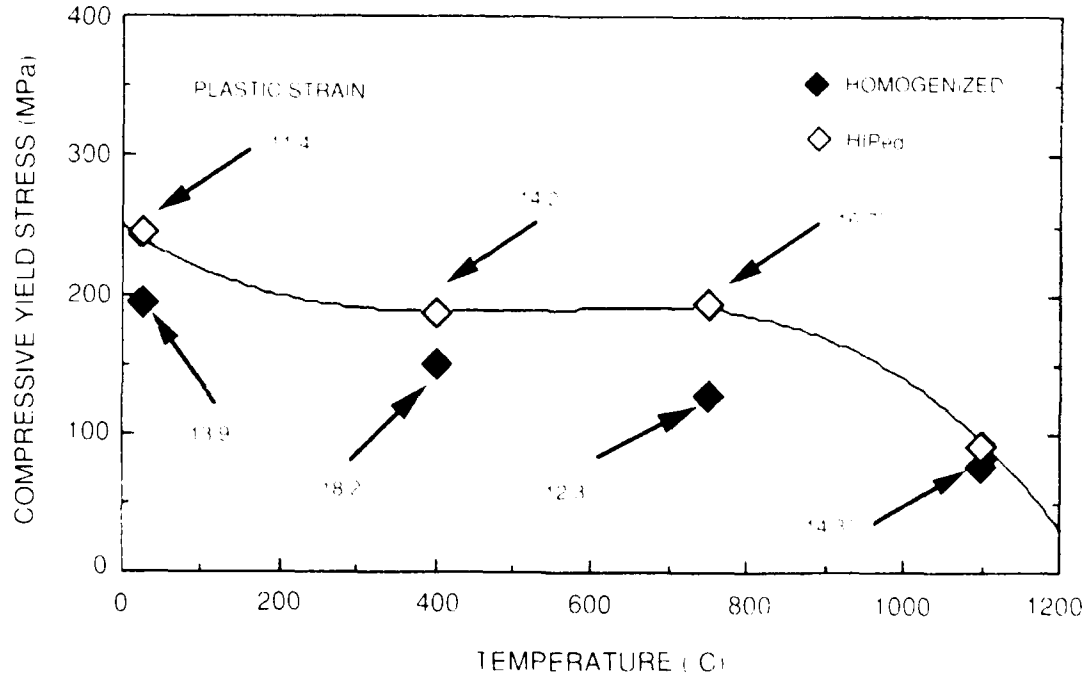

Figure 11 Temperature dependence of yield stress for Fe-modified $L1_2$-type Al_3Ti.

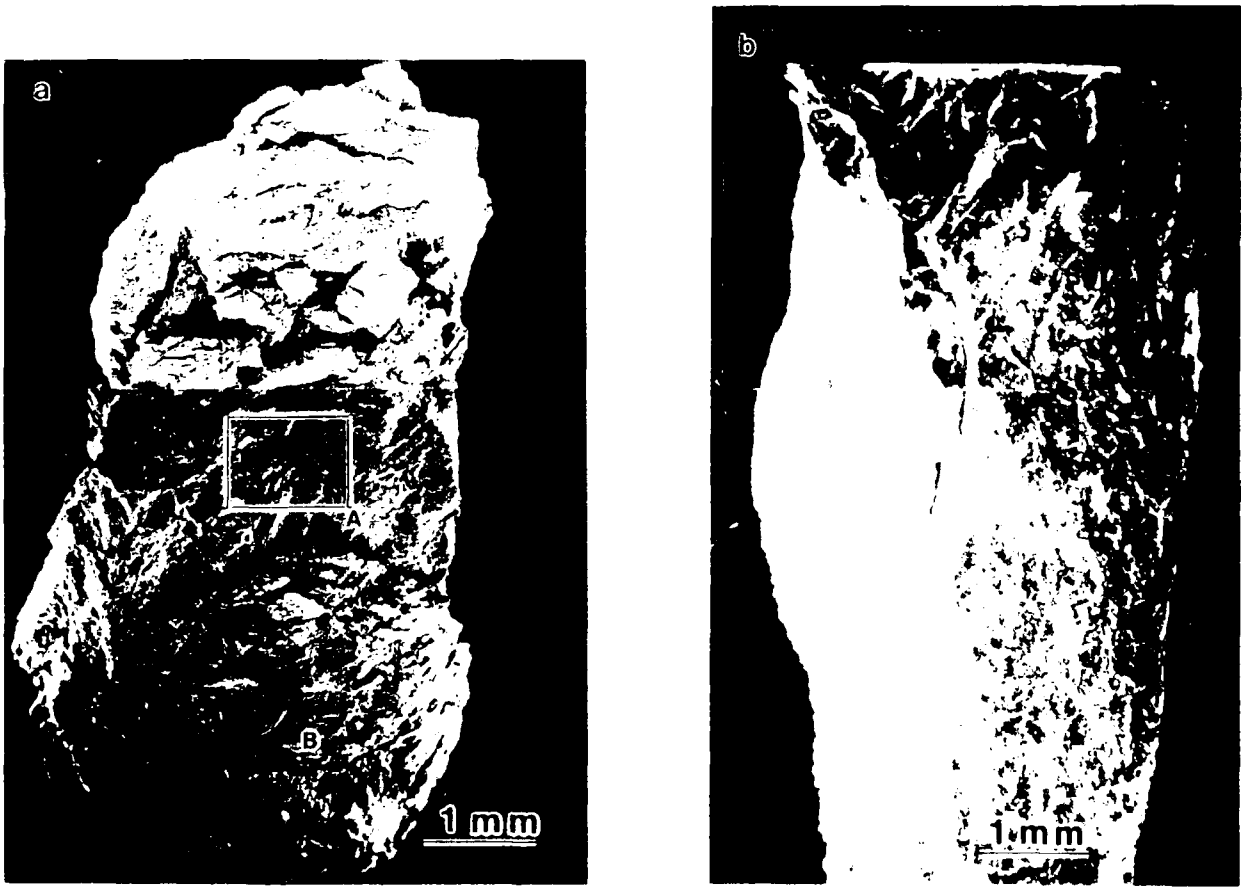

Figure 12 Deformed specimens in compression at room temperature. (a) annealed for homogenization; (b) HIPed.

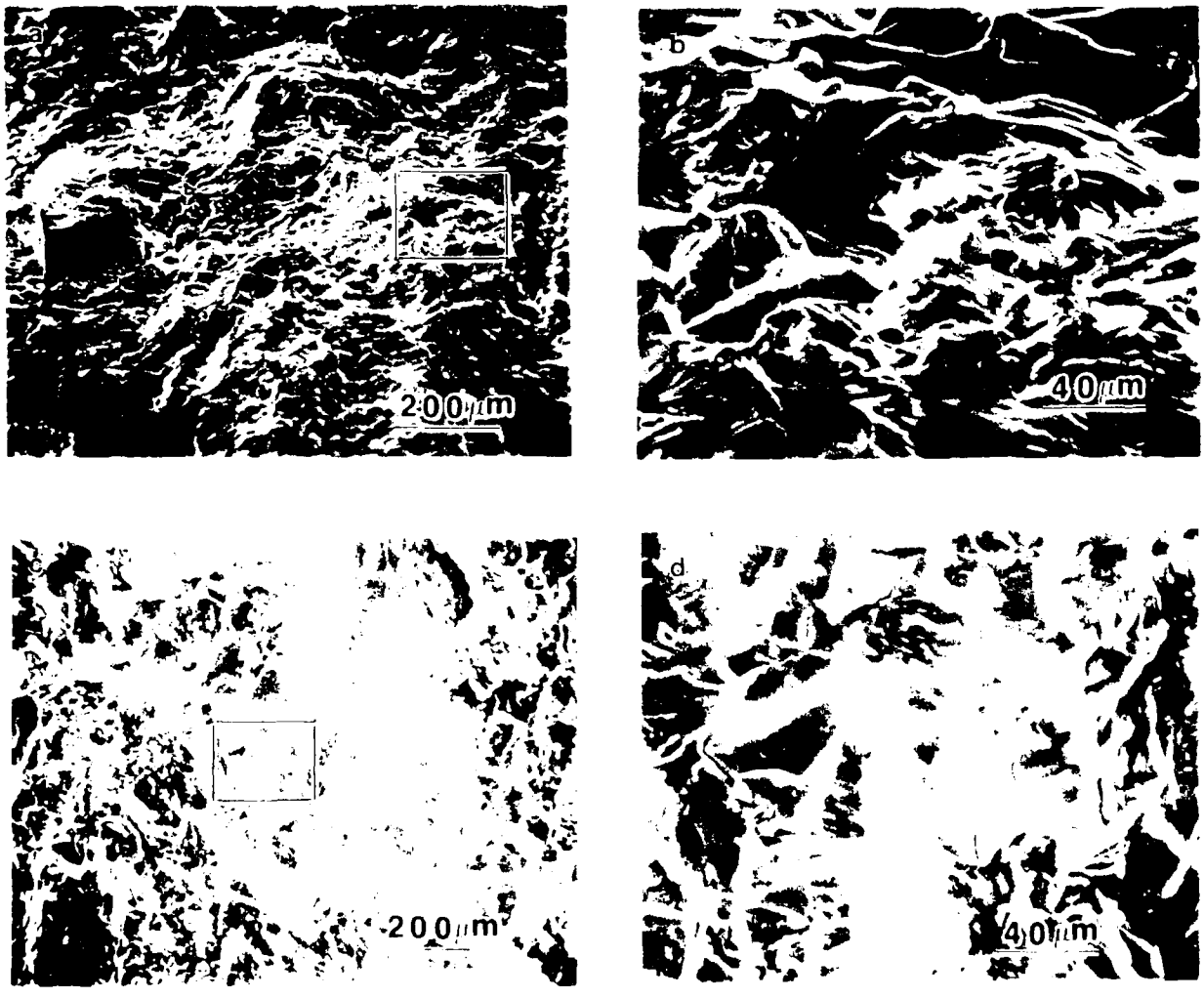

Figure 13 High magnification scanning electron micrographs taken from homogenized and HIPed specimens deformed at room temperature. (a) region A of Figure 3 (a); (b) framed region of Figure 4 (a); (c) a central region of Figure 3 (b); and (d) framed region of Figure 4 (c).

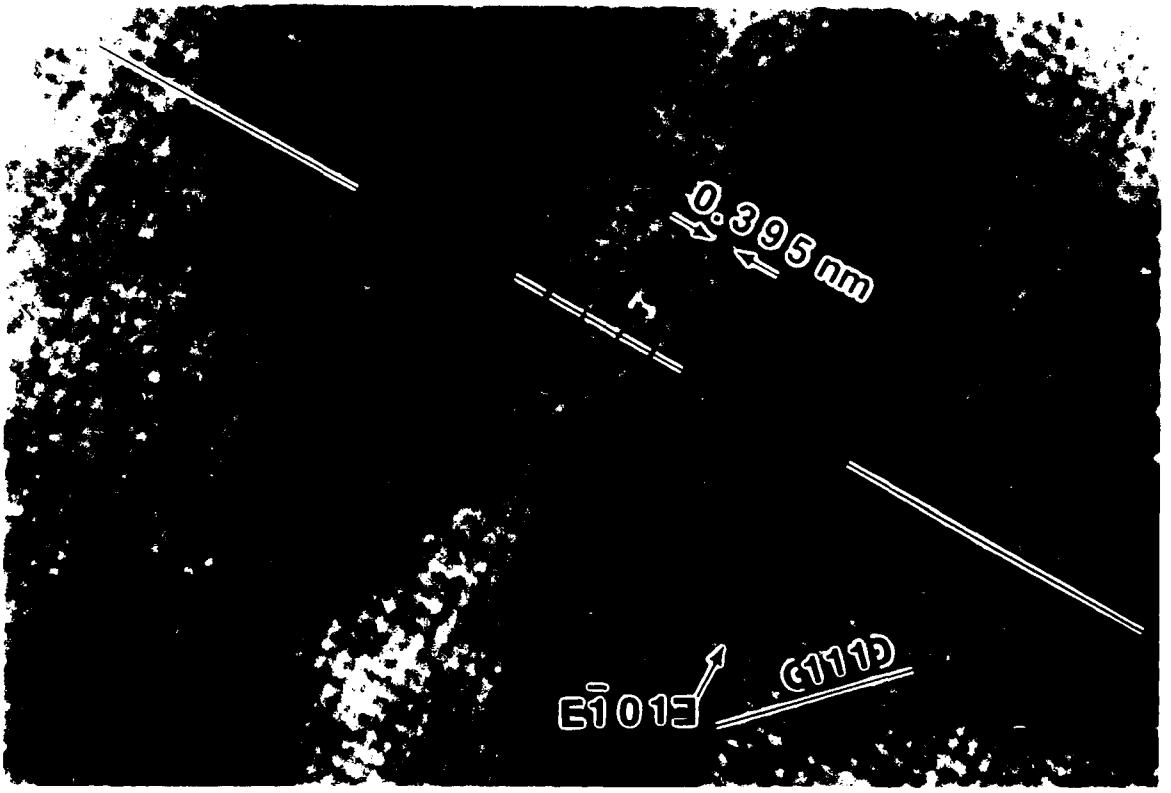

Figure 14 High-resolution electron micrograph showing pair of superlattice partial dislocations on a (111) plane having Burgers vector 1 2 [101]. Foil plane is (001). Solid lines are on atom plane; dotted lines are between atom planes. Dislocation cores are located near the center between the ends of the lines.

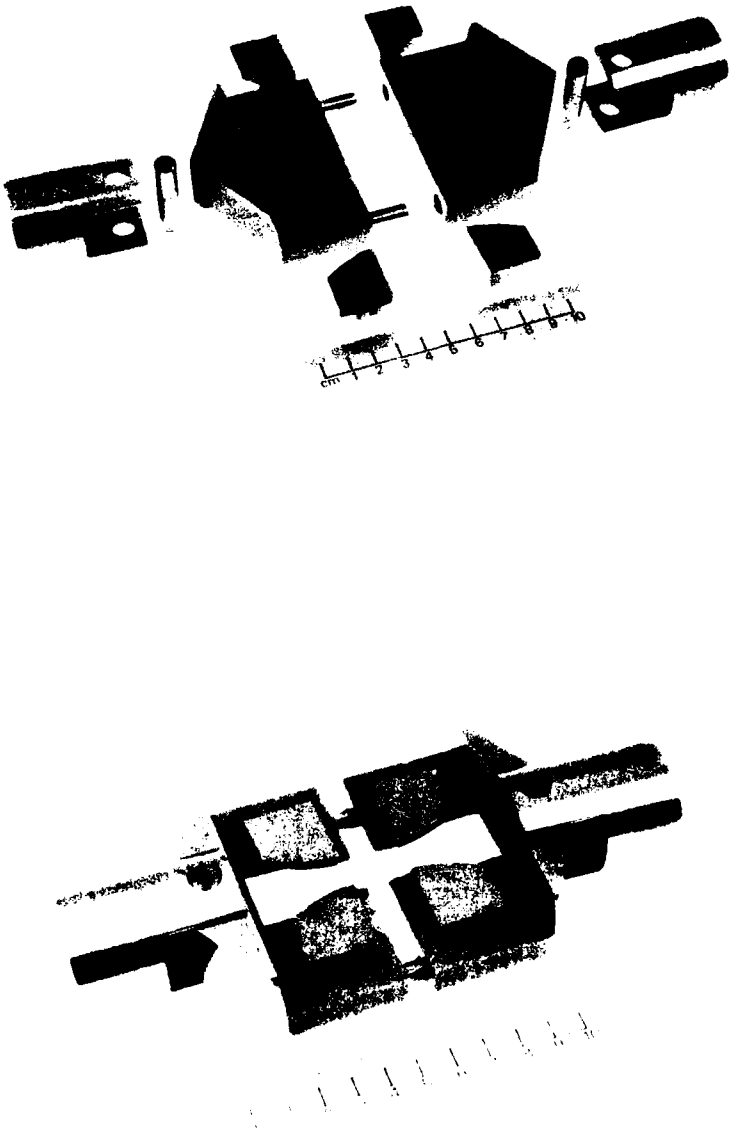

Fig. 15 Assembled and Exploded Views of Tensile/Compressive/Fatigue Fixture for Brittle Materials.